Production of dual species Bose–Einstein condensates of ^{39}K and ^{87}Rb[*]

Cheng-Dong Mi(米成栋)[1,2],   Khan Sadiq Nawaz[1,2],   Peng-Jun Wang(王鹏军)[1,2,†],   Liang-Chao Chen(陈良超)[1,2],
Zeng-Ming Meng(孟增明)[1,2],   Lianghui Huang(黄良辉)[1,2],   and   Jing Zhang(张靖)[1,2,‡]

[1] *State Key Laboratory of Quantum Optics and Quantum Optics Devices, Institute of Opto-electronics,
Shanxi University, Taiyuan 030006, China*
[2] *Collaborative Innovation Center of Extreme Optics, Shanxi University, Taiyuan 030006, China*

We report the production of ^{39}K and ^{87}Rb Bose–Einstein condensates (BECs) in the lowest hyperfine states $|F = 1, m_F = 1\rangle$ simultaneously. We collect atoms in bright/dark magneto-optical traps (MOTs) of ^{39}K/^{87}Rb to overcome the light-assisted losses of ^{39}K atoms. Gray molasses cooling on the D1 line of the ^{39}K is used to effectively increase the phase density, which improves the loading efficiency of ^{39}K into the quadrupole magnetic trap. Simultaneously, the normal molasses is employed for ^{87}Rb. After the microwave evaporation cooling on ^{87}Rb in the optically plugged magnetic trap, the atoms mixture is transferred to a crossed optical dipole trap, where the collisional properties of the two species in different combinations of the hyperfine states are studied. The dual species BECs of ^{39}K and ^{87}Rb are obtained by further evaporative cooling in an optical dipole trap at a magnetic field of 372.6 G with the background repulsive interspecies scattering length $a_{KRb} = 34a_0$ (a_0 is the Bohr radius) and the intraspecies scattering length $a_K = 20.05a_0$.

1. Introduction

Since Bose–Einstein condensates (BECs) were firstly observed in alkali atoms,[1,2] the ultracold atomic gases have attracted much attention to study many interesting quantum phenomena, e.g., the BEC–BCS crossover, spin–orbit coupling,[3–6] Mott insulator in the optical lattice,[7–9] and ultracold chemistry.[10,11] Dual species ultracold gasses greatly expand the research area of this platform to study even more complex physical phenomena that are not accessible in a single component quantum gas, such as producing heteronuclear molecules with long dipole–dipole interaction,[15–17] creating polarons near quantum criticality,[18–20] and observation of collective dynamics of a mixture of Bose and Fermi superfluids.[21] To date, several dual Bose–Bose species have been cooled to BECs in experiments, including ^{23}Na–^{87}Rb,[22] ^{39}K–^{87}Rb,[23] ^{39}K–^{23}Na,[24] ^{41}K–^{87}Rb,[25,26] ^{88}Sr–^{87}Rb, ^{84}Sr–^{87}Rb,[27] Er–Dy,[28] and ^{133}Cs–^{87}Rb.[29,30]

Recently, more interest is directed towards the ^{39}K–^{87}Rb dual-species BECs as there is rich Feshbach resonance structure[23,31] for the precise control of the interspecies scattering length in low magnetic field. Nevertheless, there are many difficulties in achieving the BEC of ^{39}K. First, its negative background scattering length[32] inhibits the achievement of the BEC state. Second, the unresolved excited-state hyper-

fine structure of ^{39}K[33] makes the standard sub-Doppler laser cooling less efficient. Third, the strong light-assisted losses of the dual species in the initial double MOTs stage[34] result in a poor loading. All of these factors make the achievement of ^{39}K–^{87}Rb dual-species BECs to be a challenging task.

In this paper, we report the experimental route to overcome these difficulties, and finally obtain the BECs of ^{39}K and ^{87}Rb in the lowest hyperfine states $|F = 1, m_F = 1\rangle$ simultaneously. Previously,[23] the ^{39}K–^{87}Rb BECs were achieved with bright molasses on the D2 line in the $|F = 1, m_F = -1\rangle$ state with the pre-cooling being done by the microwave evaporation in the quadrupole trap and later in the quadrupole Ioffe–Pritchard configuration (QUIC) trap. However, we follow a modified route to achieve the dual species condensate in the $|F = 1, m_F = 1\rangle$ state using the gray molasses on the D1 line and the pre-cooling by the microwave evaporation in an optically plugged magnetic trap. At the three-dimensional MOT phases, a dark spontaneous optical force trap (dark SPOT)[35] is used to load the ^{87}Rb atoms in the $|F = 1\rangle$ state in the central part without repumping beams, and a bright MOT loads the ^{39}K atoms at the same time. This scheme mitigates the atoms loss resulted from the inelastic collisions and the light-induced loss of different species in the MOT loading stage. To effectively cool the ^{39}K, the gray molasses cooling[36–39] on D1

line is used after the loading stage in the magneto-optic trap. The obstacle of negative background scattering length is overcome by tuning the ^{39}K scattering length to $a_{K} = 20.05a_0$ by using an external homogeneous magnetic field at 372.6 G near a broad Feshbach resonance centered at 403.4 G, where it is positive to facilitate sympathetic cooling below 1 μK with the background interspecies scattering length $a_{KRb} = 34a_0$ (a_0 is the Bohr radius) during the final evaporation step in the optical dipole trap. Using this scattering length improves the density of ^{39}K due to the sympathetic cooling compared to the case cooling the ^{39}K alone.

2. The ^{39}K and ^{87}Rb double MOT

The experimental setup is shown in Fig. 1, which has been used for the creation of ^{87}Rb BEC in Refs. [40,41]. The ^{87}Rb and ^{39}K atoms are first simultaneously cooled and trapped in the 2D MOT chamber to form an atomic beam. This beam is then pushed to the science chamber (at much lower pressure of 10^{-9} Pa) with the help of a push beam containing 4 frequencies. In the science chamber, the ^{39}K atoms are collected in a 3D MOT while the ^{87}Rb atoms are collected in a dark SPOT MOT to reduce the loss of ^{39}K atoms. We also tried the double dark SPOT MOT to further reduce the light assisted losses, however the ^{39}K dark SPOT MOT did not work. This

could be due to the use of a single (unbalanced) hollow repumping beam in contrast to the use of four hollow repumping beams (balancing each other in the opposite direction) used in Ref. [42]. Since the ^{87}Rb does not need a high power repumping beam (compared to the ^{39}K which needs almost the same power as that of the trapping/cooling beams due to its narrowly spaced excited state hyperfine splitting), we do not need to balance the single hollow repumping beam for the ^{87}Rb dark SPOT MOT. The different powers and frequencies used in the push beam and the two MOT stages are listed in Table 1 while Fig. 2 gives the definitions of the detunings.

Table 1. The detunings and powers of the different laser beams during the MOT loading ($\Gamma \simeq 6$ MHz).

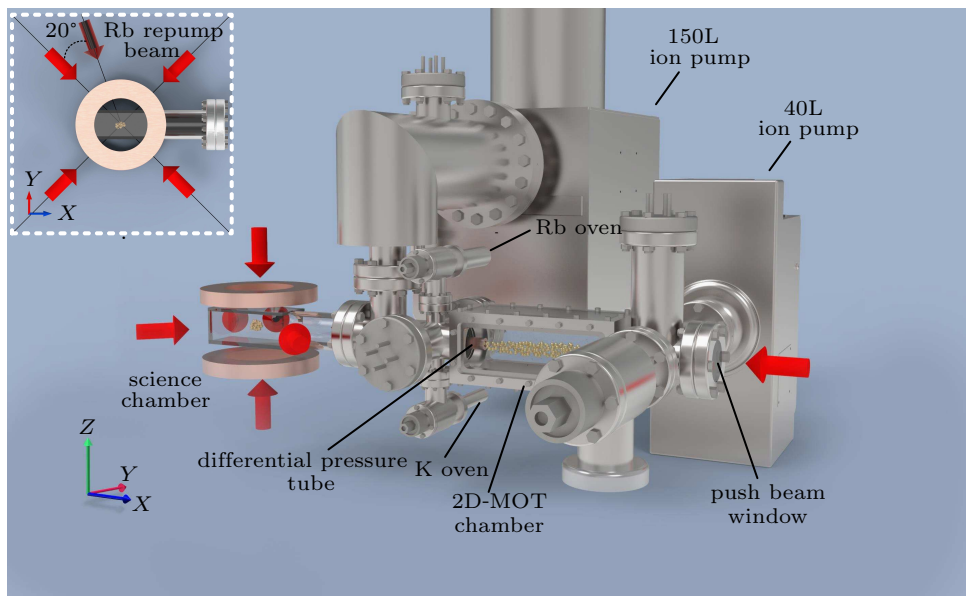|	Laser beam	Detuning	Power (mW)
2D MOT	^{87}Rb cooling	-1.48Γ	90
	^{87}Rb repumping	-0.9Γ	10
	^{39}K cooling	-4.8Γ	191
	^{39}K repumping	-2.6Γ	159
Push beams	^{87}Rb push 1	-1.48Γ	4
	^{87}Rb push 2	$+2.5\Gamma$	1
	^{39}K push 1	-4.8Γ	15
	^{39}K push 2	-0.83Γ	4
3D MOT	^{87}Rb depumping	-1.7Γ	1.5
	^{87}Rb cooling	-2.65Γ	160
	^{87}Rb repumping (dark)	-0.9Γ	9.5
	^{39}K cooling	-6Γ	213
	^{39}K repumping	-3.7Γ	177

Fig. 1. The experimental setup for the dual ^{39}K and ^{87}Rb BECs showing the two MOT cells and the ion pumps for each chamber. The Rb and K sources (at 40 °C and 45 °C, respectively) supply atoms into the 2D MOT chamber. The science chamber (enclosed by the quadrupole/Feshbach coils) collects the atoms in the 3D MOT from the push beams assisted atomic flux coming from the 2D MOT via a differential pressure tube. The inset shows the top view of 3D MOT, four horizontal MOT beams and a hollow Rb repumping beam are visible.

In the 3D MOT, there are six solid MOT laser beams (2.5 cm diameter). Each of these six beams carries the Rb and K cooling and the repumping light only for K, as shown in the insert image in Fig. 1. To produce the dark region in

^{87}Rb dark SPOT, an opaque disk with a diameter of 10 mm is used to cast a shadow at the center of the ^{87}Rb repumping beam. The center of the hollow repumping beam is filled with a depumping beam (shown in Fig. 2(b)). The repumping +

depumping beam is delivered to the 3D MOT separately from the six MOT beams and thus the ^{87}Rb atoms are trapped at the trap center in $|F = 1\rangle$ state out of the cooling cycle. The depumping beam further depletes the atomic $|F = 2\rangle$ state in the center of the MOT by optical pumping atoms to the $|F = 1\rangle$ state. The dark SPOT MOT significantly improves the simultaneous loading of both species with reduced light assisted

losses.[34] The magnetic field gradient in the 3D MOT stage is 4 G/cm along the z-axis which is provided by a pair of coils in the anti-Helmholtz configuration as shown in Fig. 1.[43] The same coils provide the homogeneous magnetic field for Feshbach resonance when the current direction in one of the coils is changed.
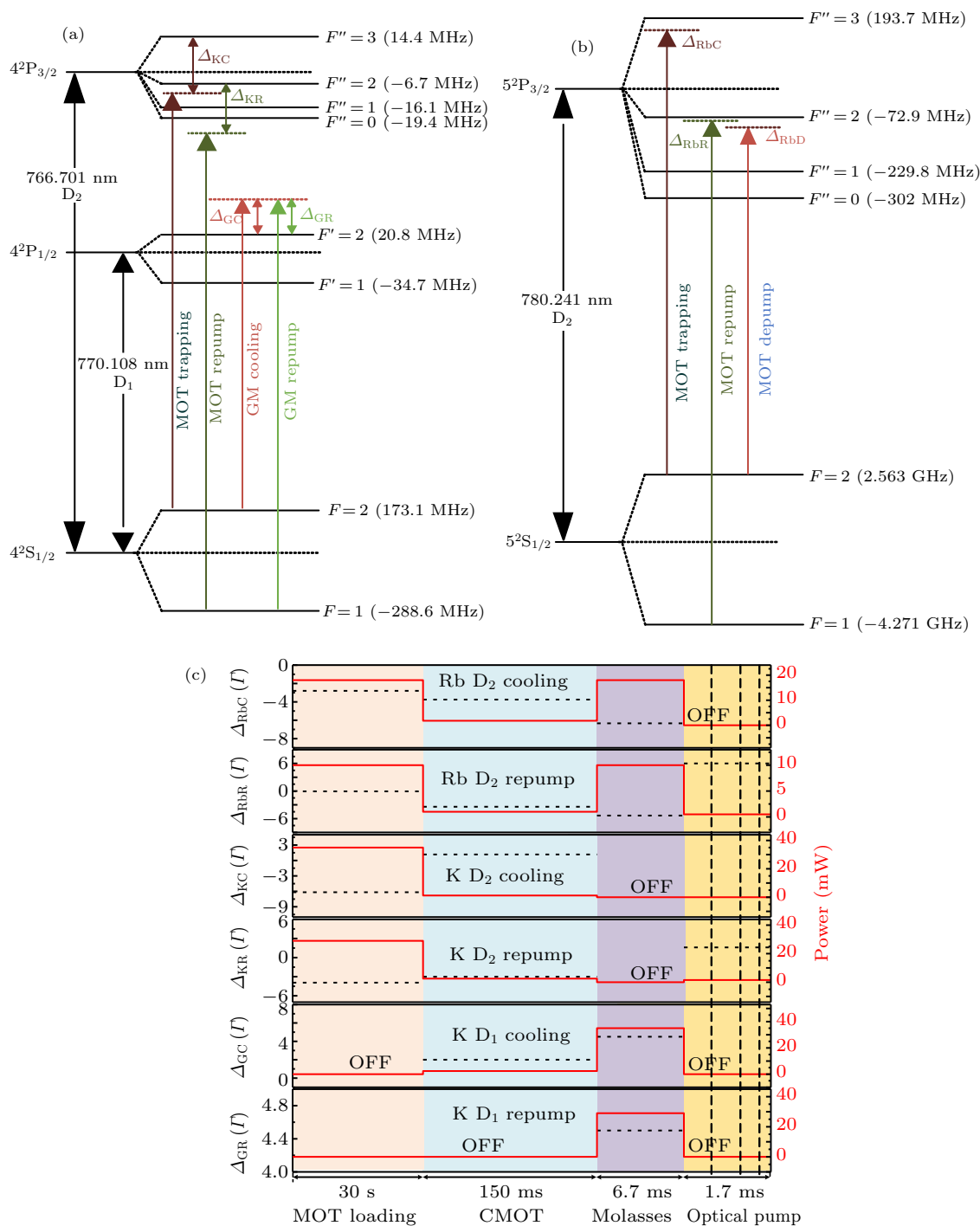

Fig. 2. Energy level diagram of ^{39}K (a) and ^{87}Rb (b), and the time sequence of the detunings and powers of each laser. (a) The Δ_{KC} and Δ_{KR} are the detunings of the trapping and repumping laser from the atomic transitions shown in the D2 line (766.7 nm) of ^{39}K. Similarly Δ_{GC} and Δ_{GR} are the GM cooling and repumping laser detunings from the transitions shown in the D1 line (770.1 nm). (b) Δ_{RbC}, Δ_{RbR}, and Δ_{RbD} are the detunings of the trapping, repumping, and depumping laser, respectively from the transitions shown in the D2 line (780.2 nm) of ^{87}Rb. (c) The time sequence of the powers (red solid lines in the right vertical axis) and detunings (black dashed lines in the left vertical axis) of the respective lasers is shown. The duration of each step of the experiment is shown on the horizontal axis.

The setup for the MOT lasers is presented in Fig. 3. For ^{87}Rb, the cooling and repumping light for the D2 line are generated by separate lasers due to large ground state hyperfine splitting of 6.8 GHz, and then frequency tuned by double-passed AOMs. The cooling beam is then amplified by a tapered amplifier (Rb-TA), as shown in Fig. 3(a). For ^{39}K, a single master laser can generate the cooling and repumping light due to the smaller ground state hyperfine splitting of 461 MHz.

We use two master lasers, one for the MOT on D2 line and the other one for the gray molasses on D1 line. The cooling beams from both the master lasers are first combined together and then amplified by an injection locked laser. A similar setup amplifies the ^{39}K repumping light and all of these are then amplified together by a single tapered amplifier (K-TA), as shown in Fig. 3(b). This design for the ^{39}K guarantees the perfect collimation of the D2 and D1 line laser beams.
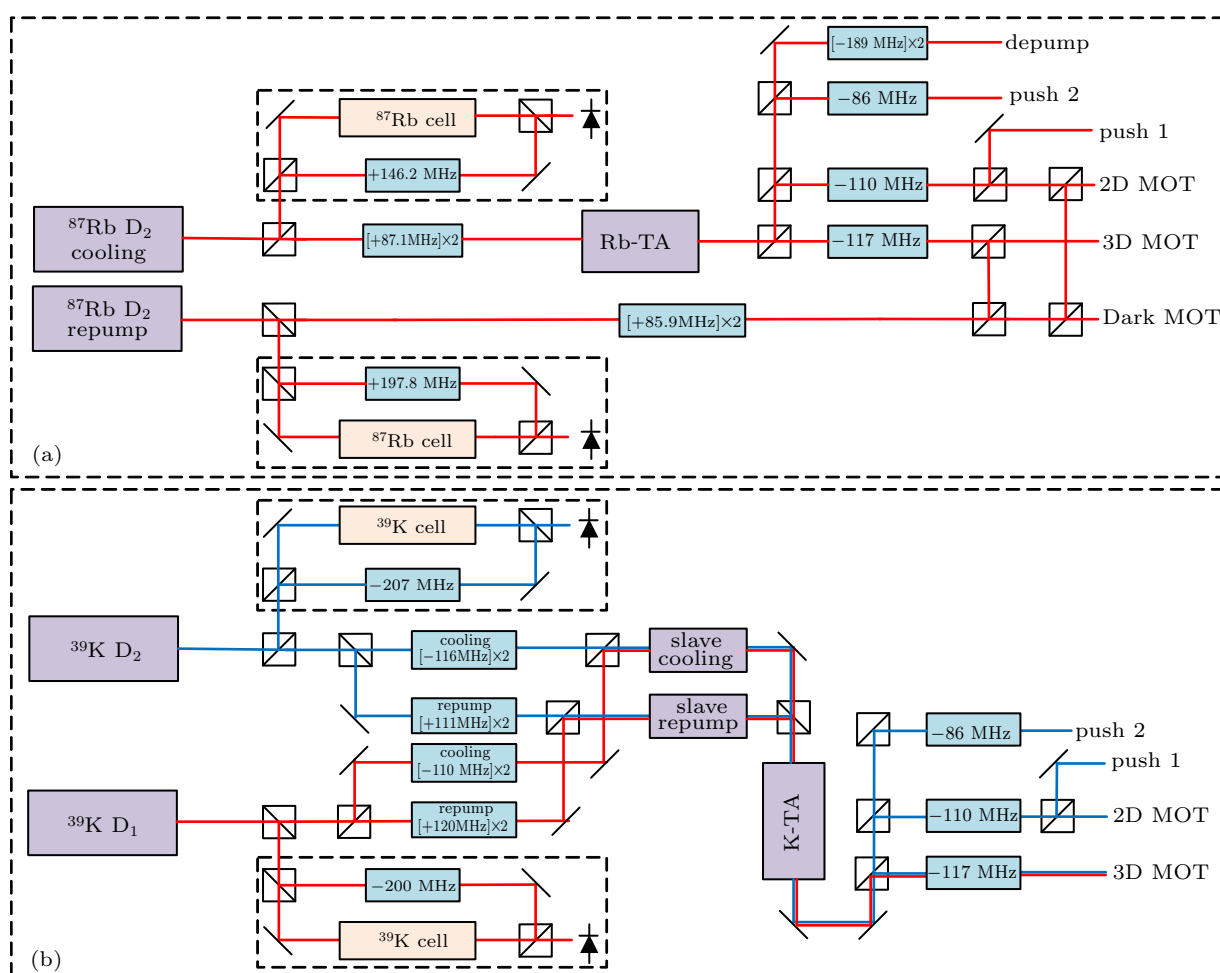

Fig. 3. The optical setup and frequency shifting and locking schemes of the (a) ^{87}Rb cooling and repumping lasers and (b) the ^{39}K D1 and D2 cooling and repumping lasers. The ^{87}Rb repumping laser does not need amplification while all of the remaining lasers are amplified by tapered amplifiers (TAs) or injection locked lasers.

The compressed MOT (CMOT) step follows the MOT loading step by increasing the magnetic field strength to 22 G/cm (duration 150 ms). The fine tuning of the laser parameters during the CMOT reduces the radiation pressure which together with the high magnetic field increases the density of the atomic sample. The repumping + depumping beam for ^{87}Rb is now blocked and the repumping light is delivered to the atoms through the six MOT beams. The detunings and single beam power of the lasers during the CMOT are shown in Fig. 2(c).

After the CMOT, the magnetic field is completely turned off in 100 µs and we perform normal molasses for the ^{87}Rb

but D1 line gray molasses for the ^{39}K. The D1 line gray molasses[37] gives samples with higher density and atoms number compared to the previously devised schemes using the D2 line laser.[23,44] The one-photon detunings Δ_{GC} and Δ_{GR} both are blue detuned $+3.33\Gamma$ forming a Raman Λ-type system in which the dark and bright states formed by the coherent superposition of the Zeeman sub-levels in the hyperfine levels $|F = 1\rangle$ and $|F = 2\rangle$ help cool in the bright state and hold the atoms in the dark state thus avoiding the chance of reheating by scattering of photons from the GM fields. The other powers and detunings are given in Fig. 2(c). The molasses step lasts for 6.7 ms.

3. Optical pumping and MW evaporation

Right after the molasses step, the pumping stage follows where both the ^{39}K and ^{87}Rb atoms are optically pumped to the $|F = 2, m_F = 2\rangle$ states. This is done by applying a 2 G homogeneous magnetic field along the x-direction and a σ^+-polarized pump light also along the same direction. The time sequence for the optimized optical pumping of both species is as follows. The repumping light for ^{87}Rb (detuning $+6\Gamma$) remains on in the six MOT beams while the ^{39}K D2 line repumping light (detuning $+1.6\Gamma$) is turned on after the molasses step. Then after 0.5 ms, the ^{39}K D1 line pump light (on resonance) is turned on for 0.7 ms and the ^{87}Rb pump light (4Γ) for 1.1 ms. The two repumping beams stay on for additional 0.1 ms. This completes the optical pumping step.

To efficiently load the sample in the magnetic quadrupole trap, the magnetic field gradient is ramped up to 26.5 G/cm in 1 ms and held on for 10 ms and then to 62 G/cm in 200 ms and held at this field for 50 ms. Finally, the magnetic trap is further compressed to 74 G/cm in 300 ms to increase the atoms density for strong collisions in the following evaporation stage. The 20 W green laser is turned on at full power focused ($\omega_0 = 30$ μm, $1/e^2$ radius) at the center of the magnetic quadrupole trap to convert it to the optically plugged magnetic quadrupole trap.

Now, the atoms of both species can be cooled by either RF evaporation or MW evaporation of ^{87}Rb only.[45] The RF evaporation transfers the hotter $|F = 2, m_F = 2\rangle$ state atoms to other un-trapped Zeeman states of the same hyperfine level but the MW evaporation transfers the $|F = 2, m_F = 2\rangle$ state atoms to the lower hyperfine (un-trapped) $|F = 1, m_F = 1\rangle$ state. The RF evaporation evaporates both the atomic species but the MW only evaporates the ^{87}Rb atoms with sympathetic cooling of the ^{39}K atoms. This MW evaporation technique compensates for the low number of ^{39}K atoms in the sample at the cost of ^{87}Rb atoms. During the MW evaporation process, the MW frequency is scanned from 6894.7 MHz to 6855.7 MHz in 6.2 s and then to 6835.7 MHz in another 5 s. At the end of the evaporation stage, there are around 1.17×10^7 ^{39}K atoms and 4.73×10^7 ^{87}Rb atoms at about 45 μK. The magnetic field strength during the evaporation is held constant at 74 G/cm.

4. Lifetime measurement of different state mixtures

After the MW evaporation cooling, the atoms are transferred to the crossed optical dipole trap, which is made by the intersection of two 1064 nm laser beams that are frequency shifted (around 10 MHz) to avoid static interference fringes. Power in both of the dipole trap beams is ramped up from zero to 3 W in 500 ms. Simultaneously, the magnetic quadrupole trap strength is ramped down from 74 G/cm to 7 G/cm in

500 ms thus the atoms are adiabatically transferred to the optical trap. Three orthogonal pairs of Helmholtz coils are used to cancel the effect of earth (and any other stray) magnetic fields on the atoms and hold them stable at the center of the dipole trap. The dipole trap center is slightly shifted from the magnetic quadrupole trap center otherwise the green laser plugged in to the magnetic quadrupole trap center would reduce the efficient loading of the dipole trap. The green laser is turned off after the loading ramp is completed. After another 10 ms, the magnetic trap strength is brought down to zero and the dipole trap alone now holds the atoms. This completes the optical dipole trap loading.

At this stage, the number of ^{87}Rb atoms is 8.21×10^6 at 18 μK while there are 2.15×10^6 ^{39}K atoms at 21 μK. The transfer efficiency of the dipole trap from the quadrupole magnetic trap is around 20% for ^{39}K and 17% for ^{87}Rb. After the loading is complete, a background magnetic field is also stabilized at 1 G along z-direction.

A forced evaporation in the optical trap then follows. The dipole trap power is quickly reduced to 2.6 W in 30 ms to remove the hotter atoms in the wings of the crossed dipole trap, and then the power decreases again to 1.6 W in 100 ms. These operations reduce the temperature of the sample down to 8 μK. Subsequently, the ^{87}Rb atoms are firstly transferred to the $|F = 1, m_F = 1\rangle$ state adiabatically using a MW sweep of 100 ms duration. Then a resonant flash light of 1 ms length removes the residual ^{87}Rb atoms in the $|2, 2\rangle$ state. After another 1 ms of waiting, the ^{39}K atoms are also transferred adiabatically to the $|F = 1, m_F = 1\rangle$ state using an RF sweep in 100 ms and a similar flash light follows removing the remaining ^{39}K atoms in the $|2, 2\rangle$ state. The transfer efficiency is almost 95%. In this spin state preparation process, it is very important to transfer the ^{87}Rb atoms to the lower hyperfine level before ^{39}K because the ground hyperfine splitting of ^{87}Rb is larger than that of ^{39}K. Therefore, a mixture of ^{87}Rb in $|F = 1, m_F = 1\rangle$ state and ^{39}K in $|F = 2, m_F = 2\rangle$ state is more stable than the other way around which results in extreme losses due to hyperfine changing collisions.[23,26,34]

To study the loss induced by this collision mechanism, we measure the lifetime of the different spin state mixtures of the ^{39}K and ^{87}Rb atoms by holding these mixtures in the same dipole trap depth for variable times and then measuring the number of remaining atoms. In Fig. 4, the ^{39}K (a) and ^{87}Rb (b) decay curves are shown for four combinations of the hyperfine states: (1) Rb$|2, 2\rangle \oplus$ K$|2, 2\rangle$, (2) Rb$|2, 2\rangle \oplus$ K$|1, 1\rangle$, (3) Rb$|1, 1\rangle \oplus$ K$|2, 2\rangle$, and (4) Rb$|1, 1\rangle \oplus$ K$|1, 1\rangle$.

The experimental data are fitted by the function $N_0 e^{-t/\tau} + N_r$, with N_r, N_0, and t as free parameters ($N_0 + N_r$ is the initial number of atoms at $t = 0$ and N_r is the residual atom number remaining after the long holding time), as the solid lines shown in Fig. 4. The τ is the lifetime of the

species in a particular mixture. We notice that the mixture of the two species in case 2 has a very low initial ^{39}K number $N_0 = 0.97 \times 10^5$, which is one order of magnitude lower than that in other cases. This is attributed to the faster loss in the spin state transfer process for ^{39}K. For case 2, we obtain very small lifetime constants of $\tau_K = 0.8$ s and $\tau_{Rb} = 3.95$ s. We attribute this observed fast decay to the hyperfine changing collision, which can be described by the equation below:

$$^{39}K(F=1, m_F=1) + ^{87}Rb(F=2, m_F=2),$$
$$\rightarrow \, ^{39}K(F=2, m_F=2) + ^{87}Rb(F=1, m_F=1) + \Delta, \quad (1)$$
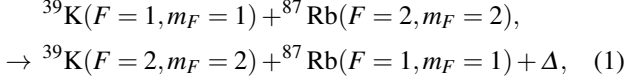
where $\Delta = h \times (6334.7 - 461.7)$ MHz $\approx k_B \times 0.306$ K. The projection of total hyperfine angular momentum $m_{F,Rb} + m_{F,K}$ is conserved in such a reaction. The released energy Δ in this process converted to the kinetic energy of the collision atoms is higher than the trapping potential of the dipole trap and results in the fast atom loss. Other hyperfine changing collisions can also happen[34] but the main contribution to the losses in our system comes from this reaction.[26,31] When the spin preparation sequence is reversed (case 3), this type of hyperfine changing collision is forbidden and longer lifetimes are observed with $\tau_K = 1.7$ s and $\tau_{Rb} = 7.92$ s.
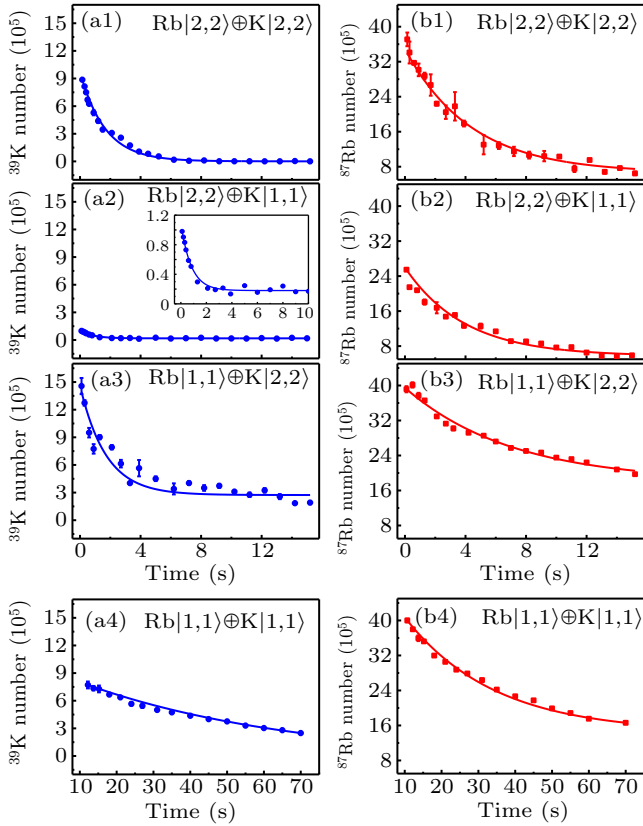

Fig. 4. The lifetimes of the various mixture states of ^{39}K and ^{87}Rb. (a) Lifetime of ^{39}K. (b) Lifetime of ^{87}Rb.

The measured most stable combination is in the case 4 with longest lifetimes $\tau_K = 28$ s and $\tau_{Rb} = 27$ s. Because there is no inelastic collision of any kind in this combination when

both species are prepared in the lowest states, the lifetime is only limited by the one-body loss induced by the collision of background gases and the photon scattering of the dipole trap beams. The ^{87}Rb and ^{39}K mixture when both in the $|2,2\rangle$ states is not as stable (case 1) as the situation when each specie is in the $|1,1\rangle$ state (case 4) because in the former case there are still some residue atoms in for example the $|2,1\rangle$ or other trappable state which can result in inelastic collisional losses. Losses from other inelastic collisions reported in Ref. [34] are also possible in this combination. Therefore, these losses result in $\tau_K = 1.65$ s and $\tau_{Rb} = 4.37$ s in case 1.

All of these lifetime measurements are done while both of the species are not condensed (at temperature of 8 μK). These decay lifetimes can be of interest for the calculation of the interspecies scattering lengths among different mixture states at ultra-cold temperatures.

5. Feshbach resonances and achievement of dual BECs

To further cool the two species, the ^{87}Rb and ^{39}K atoms are transferred to the $|F=1, m_F=1\rangle$ state after following the exact sequence of state preparation in the dipole trap and then we further perform the evaporation by ramping down the dipole trap power. During these ramp down steps, the mixture of ^{39}K ($a_K \sim -33a_0$) and ^{87}Rb ($a_{Rb} \sim 100a_0$) atoms (interspecies $a_{RbK} \sim 34a_0$) is cooled by evaporation in the presence of a homogeneous magnetic field of 1 G. The first ramp down takes 300 ms and the power in the dipole trap beams is reduced to 0.7 W. In another ramp down lasting for 1 s, the power in the dipole trap beams is reduced to 0.35 W. In the third ramp down, the dipole trap power in the two beams is reduced to 0.26 W in 500 ms. At this stage, the temperature of the atoms reaches below 1 μK. At this temperature, we measure the inter- and intra-species Feshbach resonances by scanning the external magnetic field along z-direction provided by the pair of coils in the Helmholtz configuration (shown in Fig. 1). The resonances are detected as an enhancement of atoms loss.[46–48] Figure 5 shows the results of the remaining atom number of both species after holding time of 200 ms for different magnetic field values.

Figure 5(a) shows two ^{39}K intra-species resonances (25.9 G, 403.4 G) and a single ^{87}Rb-^{39}K inter-species resonance (318.3 G) recorded by measuring the number of ^{39}K atoms after holding the two species in the magnetic field inside the dipole trap for 200 ms (including 20 ms ramp up time of the magnetic field). The corresponding number of ^{87}Rb atoms is shown in Fig. 5(b). The single inter-species resonance is clearly visible at 318.3 G from the simultaneous loss of both species. The other interesting feature in this spectrum is the increase in the ^{87}Rb atoms number (encircled) at the exact ^{39}K

intra-species resonances. This increase in the number of observed ^{87}Rb atoms is due to the reduced inter-species repulsion caused by the rapid loss of ^{39}K.
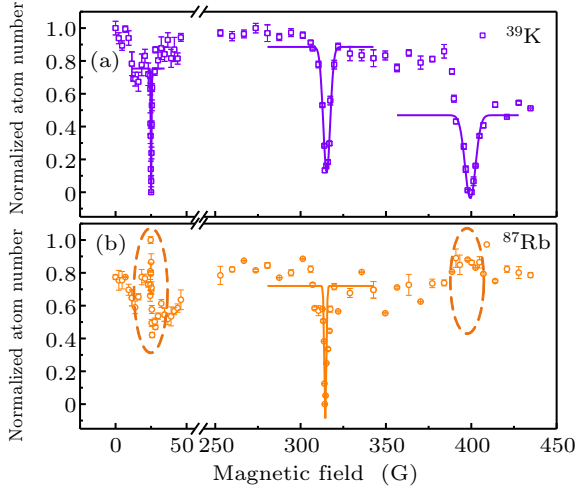

Fig. 5. The Feshbach resonance spectrum for the mixture ^{39}K and ^{87}Rb in the $|1,1\rangle$ states. Panel (a) shows the number of atoms remaining in the trap for ^{39}K and panel (b) shows that for ^{87}Rb. The two intra-species resonances at 25.9 G and 403.4 G for ^{39}K and the single inter-species resonance at 318.3 G for the mixture are presented.

When the atoms mixture is cooled to 0.8 μK, the negative background scattering length of ^{39}K significantly limits the further effective evaporation cooling. Feshbach resonance can be used to tune the scattering length to avoid this problem. Many interesting phenomena can be studied by tuning the scattering length using Feshbach resonances.[48–50] To achieve the BECs, the magnetic field of 372.6 G (which is below the ^{39}K intra-species resonance at 403.4 G) is ramped up in 20 ms and held 200 ms for the field stabilization after the previously mentioned evaporation step of both species in the $|F=1, m_F=1\rangle$ state. At this time, the scattering length of ^{39}K is $a_K = 20.05a_0$, which is obtained form the well known formula[32]

$$a(B) = a_{bg}\left(1 - \frac{\Delta}{B - B_0}\right),\qquad(2)$$

where the background scattering length $a_{bg} = -29a_0$, the Feshbach resonance position $B_0 = 403.4$ G, and the width $\Delta = -52$ G. Then the power in the dipole trap beams is reduced very slowly from 0.7 W to 0.2 W (in 2000 ms) and the final dual species BECs are produced.
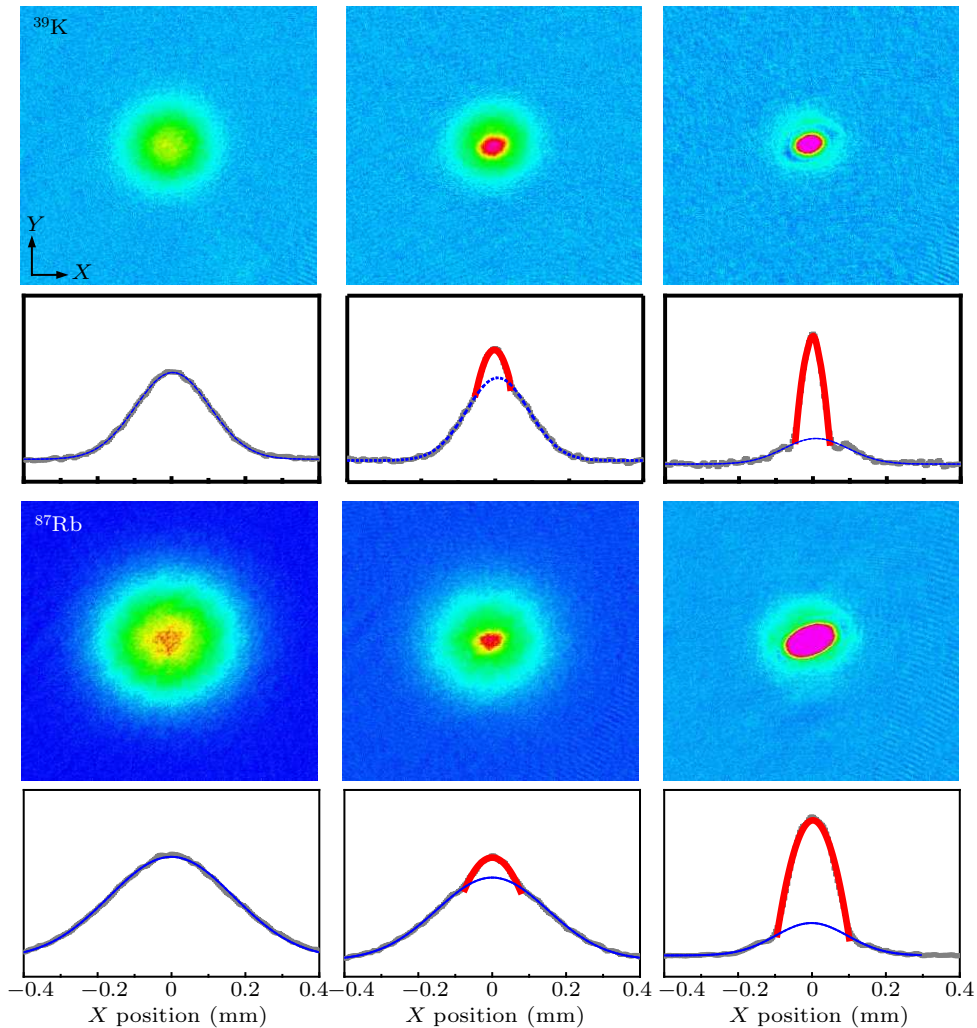

Fig. 6. Absorption images of the ^{39}K (upper row) and ^{87}Rb (lower row) atoms near the BEC critical temperature and the fits to the 1D integrated optical density along x-direction. The time of flight for these images is 20 ms for ^{39}K and 30 ms for ^{87}Rb. The field of view is 0.8 mm×0.8 mm.

To obtain the information of the BECs, the magnetic field is adiabatically ramped to 354.2 G in 30 ms and held for 100 ms for tuning the ^{39}K scattering length close to zero. Then we perform the time of flight (TOF) imaging. The dipole trap power is completely turned off to let the atom cloud to freely expand for 5 ms in high magnetic field. And then we switch off the high magnetic field and the atoms further freely expand for 20 ms for ^{39}K and 30 ms for ^{87}Rb in the background field of 1 G before the absorption imaging. The nearly pure condensates of 4.19×10^5 ^{39}K atoms and 5.11×10^5 ^{87}Rb atoms are produced.

Figure 6 shows the absorption images of the optical density of the ^{39}K and ^{87}Rb atoms, the Gaussian fitting for the thermal component, and the polynomial fitting for the condensed fraction. The bimodal character appears in the second columns for both species which means a BEC phase transition, and becomes prominent in the third column of Fig. 6 for the almost pure condensates. The first columns of Fig. 6 for both species show a single mode Gaussian fit, representing a thermal gas.

6. Achievement of ^{39}K BEC by single species evaporation

Next, we compare the evaporation efficiency of the two-species and the single-species of ^{39}K at different scattering lengths for ^{39}K. Here the scattering length a_{Rb} of ^{87}Rb is about $100a_0$ and the inter-species scattering a_{KRb} is about $34a_0$. For the two-species evaporation, we find that a BEC with high number of atoms can be obtained in the broad region of positive scattering length a_K from about $5.7a_0$ to $35.4a_0$. However, for only ^{39}K evaporation, the ^{39}K BEC can be produced at $97.3a_0$ with low atom numbers as can be seen from Fig. 7. Here we remove the ^{87}Rb atoms in the $|2, 2\rangle$ state using a flash light at 8 μK after the first two steps of evaporation in the dipole trap described above.
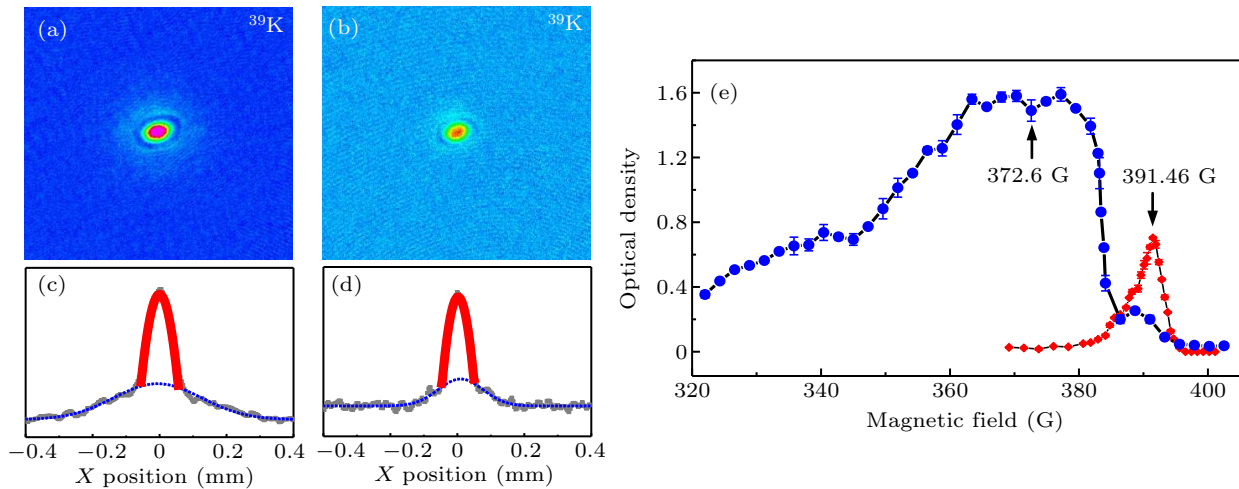

Fig. 7. Comparison of the ^{39}K BEC achieved using the two different processes. (a) Absorption image of the ^{39}K BEC achieved using the two-species evaporation performed at 372.6 G. (b) The same BEC produced using the single-species evaporation performed at 391.46 G. (c), (d) The respective poly-line fits to these BECs. (e) The optical density of the BECs as a function of the magnetic field in the two processes.

7. Conclusion

We have achieved the dual ^{39}K and ^{87}Rb BECs by utilizing various available techniques of dark SPOT MOT, D1 line gray molasses, the microwave evaporation and tuning the atomic scattering length using the Feshbach resonances. We also measure the lifetimes of these various mixture states showing interesting features especially the upper ground stretched states have shorter lifetime than the lower hyperfine stretched states. The difference in the lifetime highlights the importance of the hyperfine changing collisions in ultra-cold samples of dual species BECs. These dual BECs with rich Feshbach resonance structure and large mass imbalance can be used in various applications such as the formation of heteronuclear quantum droplets. We also show how the sympathetic cooling of ^{39}K using the ^{87}Rb atoms results in larger and denser BECs compared to the single species ^{39}K evaporative cooling.

References

[1] Anderson M H, Ensher J R, Matthews M R, Wieman C E and Cornell E A 1995 *Science* **269** 198
[2] Davis K B, Mewes M O, Andrews M R, van Druten N J, Durfee D S, Kurn D M and Ketterle W 1995 *Phys. Rev. Lett.* **75** 3969
[3] Giorgini S, Pitaevskii L P and Stringari S 2008 *Rev. Mod. Phys.* **80** 1215
[4] Wang P, Yu Z, Fu Z, Miao J, Huang L, Chai S, Zhai H and Zhang J 2012 *Phys. Rev. Lett.* **109** 095301
[5] Cheuk L W, Sommer A T, Hadzibabic Z, Yefsah T, Bakr W S and Zwierlein M W 2012 *Phys. Rev. Lett.* **109** 095302
[6] Galitski V and Spielman I B 2013 *Nature* **494** 49
[7] Wang D, Liu R, Zhu S and Scully M O 2015 *Phys. Rev. Lett.* **114** 043602
[8] Chen L, Wang P, Meng Z, Huang L, Cai H, Wang D, Zhu S and Zhang J 2018 *Phys. Rev. Lett.* **120** 193601

[9] Wang P, Chen L, Mi C, Meng Z, Huang L, Nawaz K S, Cai H, Wang D, Zhu S and Zhang J 2020 *npj Quant. Inf.* **6** 18

[10] Liu Y, Hu M, Nichols M A, Grimes D D, Karman T, Guo H and Ni K 2020 *Nat. Phys.* **16** 1132

[11] Nawaz K S, Chen L, Mi C, Chen L, Meng Z, Huang L, Wang P and Zhang J 2020 *Phys. Rev. A* **102** 053326

[12] Grimm R 2019 *Few-Body Syst.* **51** 113

[13] Tung S, Jiménez-García K, Johansen J, Parker C V and Chin C 2014 *Phys. Rev. Lett.* **113** 240402

[14] Nawaz K S, Mi C, Chen L, Wang P and Zhang J 2019 *Chin. Phys. Lett.* **36** 043201

[15] Bohn J L, Rey A M and Ye J 2017 *Science* **357** 1002

[16] Ospelkaus S, Ni K K, Wang D, de Miranda M H G, Neyenhuis B, Quéméner G, Julienne P S, Bohn J L, Jin D S and Ye J 2010 *Science* **327** 853

[17] Park J W, Will S A and Zwierlein M W 2015 *Phys. Rev. Lett.* **114** 205302

[18] Schirotzek A, Wu C, Sommer A and Zwierlein M W 2009 *Phys. Rev. Lett.* **102** 230402

[19] Kohstall C, Zaccanti M, Jag M, Trenkwalder A, Massignan P, Bruun G M, Schreck F and Grimm R 2012 *Nature* **485** 615

[20] Yan Z Z, Ni Y, Robens C and Zwierlein M W 2020 *Science* **368** 190

[21] Ferrier-Barbut I, Delehaye M, Laurent S, Grier A T, Pierce M, Rem B S, Chevy F and Salomon C 2014 *Science* **345** 1035

[22] Wang F, Li X, Xiong D and Wang D 2015 *J. Phys. B: At. Mol. Opt. Phys.* **49** 015302

[23] Wacker L, Jørgensen N B, Birkmose D, Horchani R, Ertmer W, Klempt C, Winter N, Sherson J and Arlt J J 2015 *Phys. Rev. A* **92** 053602

[24] Schulze T A, Hartmann T, Voges K K, Gempel M W, Tiemann E, Zenesini A and Ospelkaus S 2018 *Phys. Rev. A* **97** 023623

[25] Modugno G, Modugno M, Riboli F, Roati G and Inguscio M 2002 *Phys. Rev. Lett.* **89** 190404

[26] Thalhammer G, Barontini G, De Sarlo L, Catani J, Minardi F and Inguscio M 2008 *Phys. Rev. Lett.* **100** 210402

[27] Pasquiou B, Bayerle A, Tzanova S M, Stellmer S, Szczepkowski J, Parigger M, Grimm R and Schreck F 2013 *Phys. Rev. A* **88** 023601

[28] Trautmann A, Ilzhöfer P, Durastante G, Politi C, Sohmen M, Mark M J and Ferlaino F 2018 *Phys. Rev. Lett.* **121** 213601

[29] Lercher A D, Takekoshi T, Debatin M, Schuster B, Rameshan R, Ferlaino F, Grimm R and Nägerl H C 2011 *Eur. Phys. J. D* **65** 3

[30] McCarron D J, Cho H W, Jenkin D L, Köppinger M P and Cornish S L 2011 *Phys. Rev. A* **84** 011603

[31] Simoni A, Zaccanti M, D'Errico C, Fattori M, Roati G, Inguscio M and Modugno G 2008 *Phys. Rev. A* **77** 052705

[32] D'Errico C, Zaccanti M, Fattori M, Roati G, Inguscio M, Modugno G and Simoni A 2007 *New J. Phys.* **9** 223

[33] Prevedelli M, Cataliotti F S, Cornell E A, Ensher J R, Fort C, Ricci L, Tino G M and Inguscio M 1999 *Phys. Rev. A* **59** 886

[34] Marcassa L G, Telles G D, Muniz S R and Bagnato V S 2000 *Phys. Rev. A* **63** 013413

[35] Ketterle W, Davis K B, Joffe M A, Martin A and Pritchard D 1993 *Phys. Rev. Lett.* **70** 2253

[36] Nath D, Easwaran R K, Rajalakshmi G and Unnikrishnan C S 2013 *Phys. Rev. A* **88** 053407

[37] Salomon G, Fouche L, Wang P, Aspect A, Bouyer P and Bourdel T 2013 *Europhys. Lett.* **104** 63002

[38] Sievers F, Kretzschmar N, Fernandes D R, Suchet D, Rabinovic M, Wu S, Parker C V, Khaykovich L, Salomon C and Chevy F 2015 *Phys. Rev. A* **91** 023426

[39] Shi Z, Li Z, Wang P, Meng Z, Huang L and Zhang J 2018 *Chin. Phys. Lett.* **35** 123701

[40] Chen L, Meng Z and Wang P 2017 *Acta Phys. Sin.* **66** 083701 (in Chinese)

[41] Yang G, Chen L, Mi C, Wang P and Zhang J 2018 *Acta Sin. Quantum Opt.* **24** 156

[42] Wang H, Gould P L and Stwalley W C 1995 *Phys. Rev. A* **53** R1216

[43] Fan H, Wang P and Zhang J 2015 *Acta Sin. Quantum Opt.* **21** 351

[44] Landini M, Roy S, Carcagní L, Trypogeorgos D, Fattori M, Inguscio M and Modugno G 2011 *Phys. Rev. A* **84** 043432

[45] Campbell R L D, Smith R P, Tammuz N, Beattie S, Moulder S and Hadzibabic Z 2010 *Phys. Rev. A* **82** 063611

[46] Wang P, Fu Z, Chai S and Zhang J 2011 *Chin. Phys. B* **20** 103401

[47] Gerken M, Tran B, Häfner S, Tiemann E, Zhu B and Weidemüler M 2019 *Phys. Rev. A* **100** 050701

[48] Zhang B, Li F, Deng S and Wu H 2019 *Acta Sin. Quantum Opt.* **25** 413

[49] Wang J, Pan J, Cui X and Yi W 2020 *Chin. Phys. Lett.* **37** 076701

[50] Yao R, Sun Z, Zhou S and Wang Y 2018 *Chin. Phys. B* **27** 016703